Chemical bonding analysis in $Ti_{1-x-y}Al_xTa_yN$ solid solutions

S. V. Eremeev* and A. R. Shugurov

Institute of Strength Physics and Materials Science, 634055 Tomsk, Russia

E-mail: eremeev@ispms.tsc.ru

Abstract

A comprehensive study of the evolution of electronic structure and chemical bonding in disordered $Ti_{1-x}Al_xN$ and $Ti_{1-x-y}Al_xTa_yN$ systems was performed by means of *ab initio* density functional theory calculations using crystal orbital Hamilton population technique. Progressive changes in the character of interatomic chemical bonding were revealed when sequentially alloyed TiN with Al and Ta. Alloying TiN with Al leads to the change in the Ti-N bonding character from ionic to covalent, whereas Al-N bonds being strongly ionic. The following alloying of $Ti_{1-x}Al_xN$ solid solutions with Ta results in a significant reduction of the ionicity of the Al-N bonds, while retaining the covalency of the Ti-N bonds. In addition, alloying with Ta introduces metallic character of chemical bonding in $Ti_{1-x-y}Al_xTa_yN$, with the degree of metallicity increasing with growing Ta concentration. The gain in metallicity was found to be provided not only by Ta-Ta bonds, which make the main contribution, but also by Ta-N bonds, which have covalent-metallic character. A strong dependence of bonding energies in $Ti_{1-x}Al_xN$ and $Ti_{1-x-y}Al_xTa_yN$ on local atomic surrounding was found.

*To whom correspondence should be addressed

Introduction

Titanium nitride (TiN) is currently used as a structural and functional material in a variety of applications because of its unique properties.[1,2] First of all, TiN has high hardness, wear and corrosion resistance as well as high thermal stability, which are of crucial importance for protective and decorative coatings.[3,4] In addition, it is characterized by good diffusion barrier properties, low electrical resistivity, increased optical reflectance[5,6] and compatibility with complementary metal-oxide-semiconductor (CMOS) processes, that makes it promising for diffusion barrier and gate applications,[7] solar cell[8] and infrared reflector[9,10] applications as well as a coating for electrode materials in lithium-ion batteries.[11–13] Recently, TiN thin films were also suggested as alternative plasmonic material,[14–18] exhibiting less loss and providing other practical advantages compared to noble metals. However, easy oxidation of TiN already at temperatures of 500–550 °C, and its inherent brittleness restrict the field of its possible application in extreme thermal and mechanical conditions.[19,20]

An effective method of increasing TiN oxidation resistance is its alloying with aluminum. Since aluminum (as titanium) can form an fcc crystal phase,[21] it substitutes for titanium in the crystal lattice of the nitride. The addition of Al to TiN coatings drastically increases their resistance to oxidation (from 500 °C to 800 °C), and also ensures the preservation of high values of hardness and wear resistance at temperatures up to 900-950 °C.[22–24] Moreover, due to their variable optical properties TiAlN-based coatings are very promising for photothermal and solar energy applications.[25,26] However, the necessity to enhance the efficiency of photothermal conversion of concentrating solar collectors claims to increase operating temperature of solar absorbers. For example, in concentrating solar power systems with gas-phase central heat receivers operating temperature can reach 1000 °C.[27] At the same time, annealing above 900 °C results in spinodal decomposition of the metastable supersaturated $Ti_{1-x}Al_xN$ solid solution into TiN- and AlN-rich cubic domains. The metastable fcc AlN domains further transform into a stable hexagonal close packed AlN wurtzite phase with a pronounced volume increase of $\sim$24%.[28] These structural transformations cause a sharp decrease in hardness of $Ti_{1-x}Al_xN$[22] as well as generation of microcracks which serve as

fast diffusion paths, dramatically decreasing the oxidation resistance of the coatings.[29] Moreover, $Ti_{1-x}Al_xN$ is fully oxidized at 1000 °C.[20] Therefore, over the past two decades intensive efforts have been directed towards finding ways to further improve the characteristics of the Ti-Al-N system.

Along with formation of hierarchical microstructures, which allow improvement of mechanical characteristics of Ti-Al-N,[30,31] the most effective way for solving this problem is the introduction of additional alloying elements into $Ti_{1-x}Al_xN$, that is, obtaining of quaternary, quinary, etc. solutions.[32,33] In particular, the addition of elements of the IV and V groups (Zr, Nb, Hf and Ta) to the $Ti_{1-x}Al_xN$ coatings is very promising. So, Zr increases the oxidation resistance of the coatings, contributing to the formation of a dense protective oxide layer on their surface.[29,34] In addition, the introduction of its small additives leads to an increase in the hardness of the coatings and the critical temperature of spinodal decomposition. Doping with Nb leads to an increase in thermal stability and ductility of $Ti_{1-x}Al_xN$ coatings, however, there is a slight decrease in their hardness.[35] Hf provides the growth of hardness and thermal stability of $Ti_{1-x}Al_xN$ coatings, whereas the effect on their oxidation resistance is ambiguous.[36] Finally, one of the most promising alloying element is Ta, which allows not only significant enhancing of the hardness, toughness and oxidation resistance of $Ti_{1-x}Al_xN$ coatings, but also increasing the temperature of formation of the AlN wurtzite phase up to 1200°C, which ensures maintaining high hardness values up to this temperature.[32,37–39]

It is well-known that the properties of the multicomponent solid solutions strongly depend even on small variations of the relative content of the constituting chemical elements.[32] To a large extent this is due to the changes in the electronic structure and chemical bonding of the transition metal nitrides caused by variations of their elemental composition. Despite the numerous experimental and theoretical investigations of the mechanical properties,[32,35,40] solar selective characteristics,[41,42] oxidation behavior,[32,38,43] biocompatibility[44,45] and thermodynamic stability[46–49] of different ternary and quaternary TiN-based solutions, the quantitative analysis of the evolution of chemical bonding of these materials at an *ab initio* level was not thoroughly addressed. In the present paper, within density functional theory (DFT) calculations, we examine the evolution

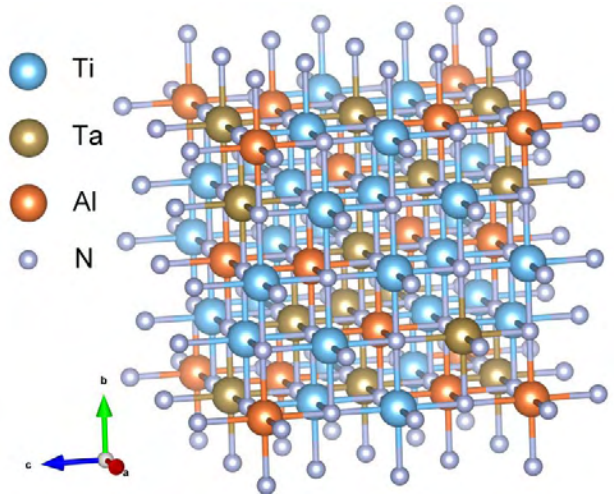

Figure 1: Supercell for disordered $Ti_{1-x-y}Al_xTa_yN$ constructed on the base of 2×2×2 cell of the cubic TiN with 25% of Al and 25% of Ta atoms randomly distributed on the Ti sublattice. The presented ball-and-stick atomic structure was created with VESTA.[50]

of electronic structure and the interatomic chemical bonding in multicomponent TiN-based solid solutions from TiN through $Ti_{1-x}Al_xN$ to $Ti_{1-x-y}Al_xTa_yN$ with different atomic ratios of Ti, Al and Ta, using crystal orbital Hamilton population formalism. We also discuss the effect of the chemical bonding on elastic properties of the TiN-based systems.

Calculation methods

The density functional theory calculations were done with the Vienna *ab initio* simulation package (VASP)[51,52] using the projector augmented wave (PAW) method.[53,54] The electron exchange-correlation functional was described by the generalized gradient approximation (GGA) in the form proposed by Perdew, Burke, and Ernzerhof (PBE).[55]

The $Ti_{1-x-y}Al_xTa_yN$ solid solutions were modeled by 2×2×2 rocksalt cubic supercells containing 64 atoms in which the metal sublattice was occupied by randomly distributed Ti, Al, and Ta atoms. As an example of such supercells, the structure containing 50% of Ti, 25% of Al and 25% of Ta atoms on the the metal sublattice is shown in Fig. Figure 1. The structure relaxation considering both the atomic positions and lattice vectors was performed by the conjugate gradient scheme until the maximum force on each atom was less than 0.001 eV/Å, and the total energy was

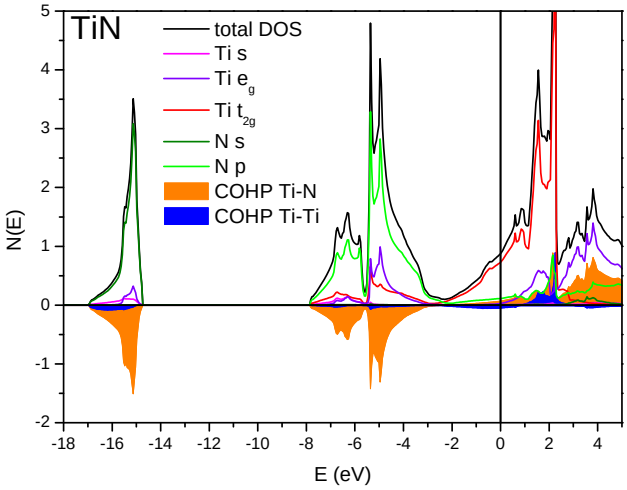

Figure 2: Total and partial DOSs for TiN and COHPs for Ti-N and Ti-Ti bonds.

converged to 10^{-6} eV with the tetrahedron method with Blöchl corrections. The Brillouin zone (BZ) integration was sampled by using a $9\times9\times9$ Monkhorst-Pack k-points grid for the calculations of relaxation and electronic structure. The elastic constants C_{ij} were calculated by an automatic procedure[56,57] implemented in VASP. The cubic elastic constants for disordered $Ti_{1-x-y}Al_xTa_yN$ solid solutions, $\widetilde{C}_{11}$, $\widetilde{C}_{12}$, and $\widetilde{C}_{44}$, were obtained by averaging as $\widetilde{C}_{11} = 1/3(C_{11}+C_{22}+C_{33})$, $\widetilde{C}_{12} = 1/3(C_{12}+C_{13}+C_{23})$, and $\widetilde{C}_{44} = 1/3(C_{44}+C_{55}+C_{66})$. Isotropic bulk B and shear G moduli were evaluated as described in Ref. 58.

To study the interatomic chemical bonding in multicomponent systems based on TiN, we used crystal orbital Hamilton population (COHP) analysis.[59] This technique adopted for plane-wave electronic structure calculations (projected COHP)[60,61] and realized in the Local Orbital Basis Suite Towards Electronic-Structure Reconstruction (LOBSTER) code[62] allows deriving an energy-resolved local bonding analysis and partitioning the band-structure energy into bonding and antibonding contributions from the PAW electronic structure calculations. Similar to the density of states (DOS), where the energy integration up to the Fermi level gives the number of electrons, the energy integration of the COHP for a pair of atoms indicates bond strength in terms of their contribution to the band structure energy.

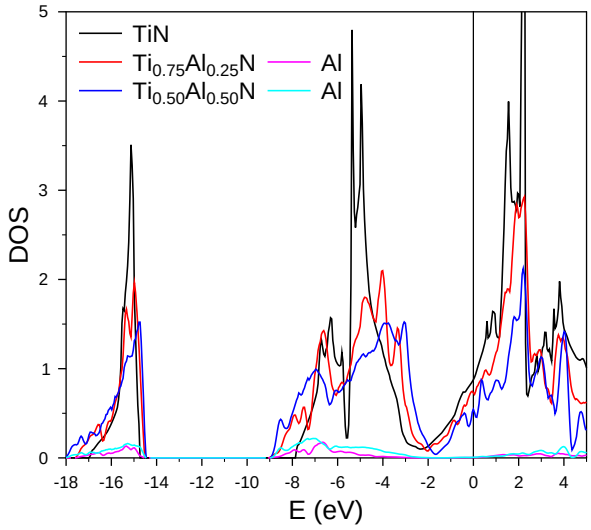

Figure 3: Total DOS of $Ti_{0.75}Al_{0.25}N$ and $Ti_{0.50}Al_{0.50}N$ in comparison with TiN total DOS and corresponding partial Al DOS.

Results and discussion

TiN belongs to NaCl-type cubic structure with the Ti atom sitting at the 1*a* (0, 0, 0) site, and the N atom at the 1*b* (0.5, 0.5, 0.5) position. The calculated equilibrium lattice parameter of titanium nitride, 4.255 Å, agrees well with the experimental value of 4.244 Å.[63] The calculated elastic constants C_{11}, C_{12}, and C_{44} equal to 613, 137, and 155 GPa, respectively, are in good agreement with the data of earlier theoretical work (610, 137, and 158 GPa)[10] and experiment (625, 165, and 163 GPa).[64]

Fig. Figure 2 shows the calculated total and partial densities of states of titanium nitride as well as COHP for the Ti-N and Ti-Ti bonds. As can be seen from the figure, in the valence band one can distinguish three energy regions: from -17 to -14.5 eV, from -8 to -2.5 eV, and from -2.5 to the Fermi level. The deep energy region is mainly contributed by *s* electrons of nitrogen, while *s* and *d* electrons of titanium participate also, in a smaller extent. The middle energy region is characterized by the strong hybridization of the Ti *d* orbitals both of e_g ($d(x^2-y^2)$, $d(z^2)$) and t_{2g} ($d(xy)$, $d(yz)$, $d(xz)$) symmetry with the N *p* orbitals. In the third DOS region the energy states are primarily contributed by the Ti t_{2g} orbitals with negligible contribution of the N *p* electrons. The strong hybridization between Ti *d* and N *p* orbitals in the middle energy region is usually

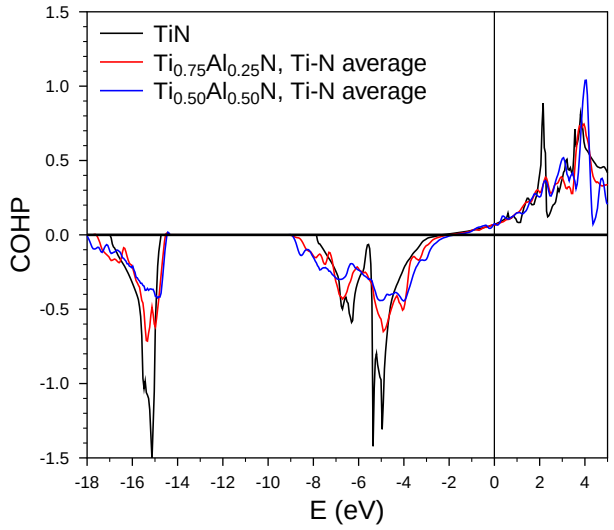

Figure 4: Average COHP for Ti-N bonds in $Ti_{0.75}Al_{0.25}N$ and $Ti_{0.50}Al_{0.50}N$ in comparison with TiN.

thought[65,66] to be responsible for ionic bonding and high strength of titanium nitride while weakly overlapped deep states almost do not contribute to Ti-N bonding. At the same time, the occupied t_{2g} states near the Fermi level are believed to contribute to metallic bonding.

At high binding energies the COHP for the Ti-N bond is negative, which indicates the bonding character of the orbitals in this energy region. At an energy of -2.34 eV Ti-N COHP changes the sign and states lying above have antibonding character. The integration of COHP (taken with the opposite sign) for occupied states gives the bond strength energy for Ti-N pair equal to 2.695 eV. It is noteworthy that a contribution to the Ti-N bonding is given not only by strongly hybridized orbitals of the middle energy region but also by weakly overlapped deep states which provide about 40% of the Ti-N bond strength. At the same time, the Ti-Ti COHP is negative over the whole occupied region, however the Ti-Ti bond strength is only 0.321 eV, i.e. it is eight times weaker as compared to Ti-N bonding.

First, the effect of aluminum alloying on the electronic structure and Ti-N bonding energy was considered. Random supercells in which aluminum atoms replace 25 and 50% of titanium atoms were constructed. The equilibrium lattice parameters obtained (normalized to the $1\times1\times1$ cubic cell) are 4.218 and 4.177 Å for $Ti_{1-x}Al_xN$ solutions with x=0.25 and 0.5, respectively,

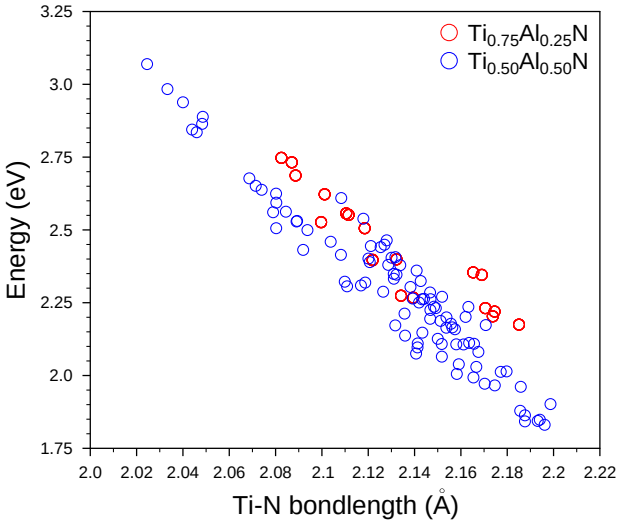

Figure 5: Dependence of bond energy of Ti-N pair on Ti-N bondlength in $Ti_{0.75}Al_{0.25}N$ (144 Ti-N bonds) and $Ti_{0.50}Al_{0.50}N$ (96 Ti-N bonds).

i.e. it is observed an almost linear decrease in the lattice parameter with increasing aluminum concentration. The atoms in the lattice are shifted from the ideal positions due to atomic relaxation. The lengths of the Ti-N bonds are equal to half of the cubic lattice parameter in pristine TiN, i.e. 2.1275 Å. With the addition of 25% aluminum in the system the Ti-N bond lengths vary from 2.0825 to 2.1851 Å. In the case of the supercell with 50% aluminum concentration the Ti-N bond lengths vary in even greater extent, from 2.0245 to 2.1986 Å.

As can be seen in Fig. Figure 3, alloying of TiN matrix with 25% of aluminum leads to substantial rearrangement of the electronic structure. The valence band in the deep and middle energy regions experiences significant broadening and smoothing of sharp DOS peaks due to Al-N hybridization. At the same time, a further increase in the concentration of aluminum up to 50% does not lead to a qualitative change in the density of states. Fig. Figure 4 shows calculated average COHP for Ti-N bonds in the $Ti_{0.75}Al_{0.25}N$ and $Ti_{0.50}Al_{0.50}N$ solid solutions. Like in pristine TiN, the states at high binding energies have the bonding character, and the states lying near the Fermi level are antibonding. However, the energy at which the COHP changes the sign shifts slightly to a less negative value with increasing aluminum concentration (-2.035 and -1.718 eV for $Ti_{0.75}Al_{0.25}N$ and $Ti_{0.50}Al_{0.50}N$, respectively). Integrating the average COHP shows a

decrease in the average energy of the Ti-N bond. In the $Ti_{0.75}Al_{0.25}N$ solution the average bond strength energy is 2.433 eV, i.e. it decreases by 10% compared to the energy of the Ti-N bond in the titanium nitride. In $Ti_{0.50}Al_{0.50}N$ the average Ti-N bond energy is reduced to 2.290 eV that corresponds to a 15% decrease compared to the original system. Herewith, the deviation of the bonding energies of the Ti-N pairs in $Ti_{0.75}Al_{0.25}N$ from the average bond strength energy is quite significant, $\sim$0.3 eV (Fig. Figure 5). The smallest energy, 2.174 eV, was found for the longest Ti-N bond length, which corresponds to the Ti-N pair with the largest number of aluminum atoms in the first coordination sphere of the nitrogen atom and in the second coordination sphere of the titanium atom, and conversely, the highest bond energy, 2.748 eV, was realized for the Ti-N pair with the smallest number of surrounding aluminum atoms, which in turn had the shortest bond length. The range of pair bond energy values increases significantly with increasing aluminum concentration. The difference between the largest and smallest values amounts $\sim$0.7 eV in $Ti_{0.50}Al_{0.50}N$, where, as noted above, variation in Ti-N bond lengths is larger also (Fig. Figure 5). It is worth noting that for the both considered Al concentrations, despite the decrease in the average Ti-N bond energy, the highest bond strength energies of Ti-N pairs (2.748 and 3.069 eV for $Ti_{0.75}Al_{0.25}N$ and $Ti_{0.50}Al_{0.50}N$, respectively) exceed the bond energy in titanium nitride (2.695 eV), that is related to inhomogeneous distortions of local bonds caused by randomly distributed Al alloying atoms. Wherein, the displacements of atoms from their ideal crystallographic positions increase with increasing Al concentration. The maximal atomic displacements in $Ti_{0.75}Al_{0.25}N$ amount $\sim$0.09 Å, whereas in $Ti_{0.50}Al_{0.50}N$ the maximal displacements are 0.12 Å for metal atoms and even reach 0.14 Å for nitrogen atoms.

In Fig. Figure 6, left panel, it is presented the total valence charge density of TiN in the (001) plane, which shows almost spherical shape of the charge distribution that corresponds to strong ionic character of the Ti-N bonds. The charge transfer from the titanium atom to the nitrogen atom calculated using the Bader method[67] amounts 2.12 *e*. In $Ti_{0.75}Al_{0.25}N$ (Fig. Figure 6, central panel), the Al-N bonds are also highly ionic, since the aluminum valence electrons are almost completely transferred to neighboring nitrogen atoms. At the same time, as can be seen from

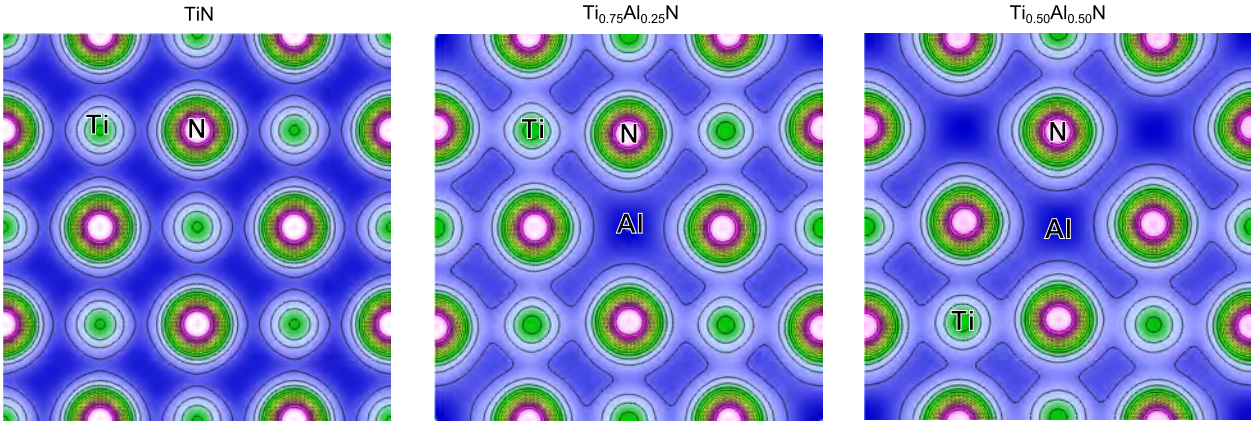

Figure 6: Charge density distribution in the (001) plane for TiN, $Ti_{0.75}Al_{0.25}N$ and $Ti_{0.50}Al_{0.50}N$.

the charge density distribution map, the charge around the Ti atoms in this case is localized along the bonds with the closest N atoms. Such charge distribution indicates an increase in the covalent component in the Ti-N bonding due to aluminum alloying. In $Ti_{0.50}Al_{0.50}N$ (Fig. Figure 6, right panel) the charge density distribution along the Ti-N bonds does not change qualitatively as compared with that of $Ti_{0.75}Al_{0.25}N$ that correlates with a relatively small variation of the average Ti-N bond strength with an increase in the Al concentration.

Modification of chemical bonds due to Al alloying leads to a change in the elastic properties of the material compared to pure TiN. Averaged $\widetilde{C}_{11}$ constants decrease by 5% and 12% in $Ti_{0.75}Al_{0.25}N$ and $Ti_{0.50}Al_{0.50}N$, respectively, as compared with TiN, whereas $\widetilde{C}_{12}$ and $\widetilde{C}_{44}$ significantly increase. $\widetilde{C}_{12}$ exceeds the C_{12} in TiN by 18% ($Ti_{0.75}Al_{0.25}N$) and 23% ($Ti_{0.50}Al_{0.50}N$). $\widetilde{C}_{44}$ increases by 16% in $Ti_{0.75}Al_{0.25}N$ and by 40% in $Ti_{0.50}Al_{0.50}N$ as compared with the corresponding elastic constant of TiN. Evaluation of elastic moduli of the ternary compositions using the calculated elastic constants showed that alloying TiN with Al results in a monotonic increase in the G/B ratio that is accompanied by a decrease in the Cauchy's pressure C_{12}-C_{44}. According to the empirical criteria of Pettifor[68] and Pugh,[69] this behavior means that $Ti_{1-x}Al_xN$ solutions become progressively less ductile with increasing x. Thus, alloying with Al leads to embritllement of TiN that is detrimental for most its applications. This behavior is associated with strong ionic character of Al-N bonds. It should be noted that this effect is substantially more pronounced at high Al concentrations. While $\widetilde{C}_{12}$-$\widetilde{C}_{44}$ and G/B of TiN are -18 GPa and 0.635, respectively, in

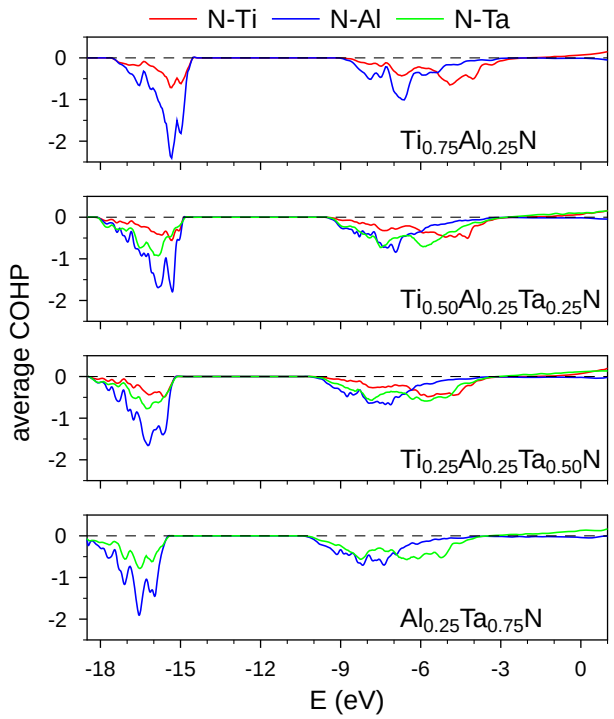

Figure 7: Average COHP for Ti-N, Al-N, and Ta-N bonds in $Ti_{0.75-y}Al_{0.25}Ta_yN$ with y varying from 0 to 0.75.

$Ti_{0.75}Al_{0.25}N$ they are -19 and 0.637, respectively, demonstrating very slight changes. In contrast, in $Ti_{0.50}Al_{0.50}N$ the Cauchy's pressure becomes 2.8 times more negative (-50 GPa), whereas the G/B ratio increases by $\sim$11% (up to 0.704).

Since there is no revealed qualitative changes in the character of the chemical bonding in $Ti_{1-x}Al_xN$ with increasing Al concentration, for consideration of quaternary $Ti_{1-x-y}Al_xTa_yN$ solutions we fix the aluminum concentration at 25%. Fig. Figure 7 shows the average COHP for the Ti-N, Al-N, and Ta-N bonds in $Ti_{0.75-y}Al_{0.25}Ta_yN$ solutions with y varying from 0 to 0.75. When $y = 0$, i.e. in $Ti_{0.75}Al_{0.25}N$, as shown above, a significant decrease in the ionicity of the Ti-N bond occurs, while the Al-N bond, as follows from the distribution of charge density, is strongly ionic. This is consistent with the form of the average COHP for Al-N, which demonstrates strongly localized character of the bonding states with sharp peaks in the deep and middle energy regions. Herewith, the hybridization of the deep N s and Al p valence states provides $\sim$50% of Al-N bond energy. With increasing the tantalum concentration in the supercell in increments of 25%, a monotonic

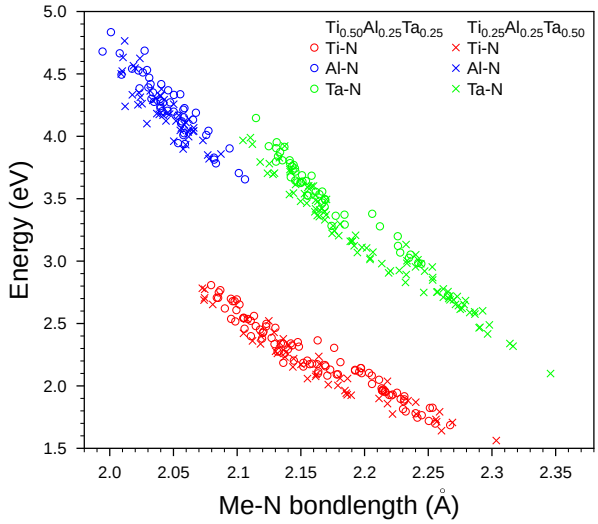

Figure 8: Dependence of bond energy of metal-N (Me-N) pair on Me-N bondlength in $Ti_{0.50}Al_{0.25}Ta_{0.25}N$ and $Ti_{0.25}Al_{0.25}Ta_{0.50}N$.

increase by about 1% of the equilibrium lattice parameter of $Ti_{0.75-y}Al_{0.25}Ta_yN$ is observed. The calculated lattice parameters are 4.218, 4.266, 4.305, and 4.344 Å in the range of y from 0 to 0.75. At the same time, a change in the average length of Al-N bonds as a function of y is not significant, showing a decrease of only half a percent in the limiting case. The deviations of the Al-N bond lengths from the average value do not exceed 0.05 Å. However, as can be seen from Fig. Figure 7, with an increase in tantalum concentration, the sharp Al-N COHP peaks become more diffuse and the average Al-N bond energy smoothly decreases: 4.321 eV in $Ti_{0.75}Al_{0.25}N$, 4.237 eV in $Ti_{0.50}Al_{0.25}Ta_{0.25}N$, 4.205 eV in $Ti_{0.25}Al_{0.25}Ta_{0.50}N$ and 4.172 eV in $Al_{0.25}Ta_{0.75}N$. Thus, in spite of the constant aluminum concentration in $Ti_{0.75-y}Al_{0.25}Ta_yN$, variation of the concentration of tantalum leads to a decrease in the strength of the Al-N bonds and their change from strongly ionic to more covalent. In addition, whereas the difference between the minimum and maximum bond energies of Al-N pairs in the ternary solutions $Ti_{0.75}Al_{0.25}N$ and $Al_{0.25}Ta_{0.75}N$ is only 0.2–0.4 eV, in the quaternary ones, due to the larger distortions of pair bonds it makes $\approx$1 eV (Fig. Figure 8). The larger distortions of the bonds in the quaternary $Ti_{0.75-y}Al_{0.25}Ta_yN$ solutions are due to significantly larger displacements of the atoms from ideal positions of the cubic structure as compared with those in $Ti_{0.75}Al_{0.25}N$. At y=0.25 the maximal atomic displacement is 0.15 Å and

it is almost twice as large for y=0.50 (0.28 Å). The smallest (largest) bond energies are obtained for the Al-N pairs, in which the number of tantalum atoms in the first neighbors of N atom is maximal (minimal). Thus, not only the number and type of neighboring atoms, but also their relative positioning affects the values of the Al-N pair bond energy in the quaternary solutions.

Partial replacement of Ti with Ta in $Ti_{0.75-y}Al_{0.25}Ta_yN$, as can be seen from Fig. Figure 7, does not change the character of Ti-N bonds, leading, however, to a decrease in the average Ti-N bond strength with increasing tantalum concentration (2.228 and 2.146 eV for y = 0.25 and y = 0.50, respectively). However, while the variation in the bond energy of Ti-N pairs in $Ti_{0.75}Al_{0.25}N$ is ≈0.5 eV, in the quaternary solutions it exceeds 1 eV (Fig. Figure 8). The variation in the Ti-N bond lengths also increases by about two times reaching ∼0.2 Å, although the average Ti-N bond length weakly depends on the concentration of tantalum, amounting to 2.163 and 2.167 Å for $Ti_{0.50}Al_{0.25}Ta_{0.25}N$ and $Ti_{0.25}Al_{0.25}Ta_{0.50}N$, respectively.

As can be seen from the average COHP for Ta-N bonds (Fig. Figure 7), for any y the Ta-N bonding has covalent-metallic character, with the degree of metallicity growing with increasing Ta concentration. With raising y, an increase in the average Ta-N bond length and a decrease in the average bond energy are observed (3.542, 3.117 and 2.921 eV for $Ti_{0.50}Al_{0.25}Ta_{0.25}N$, $Ti_{0.25}Al_{0.25}Ta_{0.50}N$ and $Al_{0.25}Ta_{0.75}N$, respectively). At the same time, the variation of the Ta-N bond strength on the configuration of the atomic environment is stronger than for Ti-N and Al-N pairs in $Ti_{0.75-y}Al_{0.25}Ta_yN$ and the difference between the minimum and maximum energies is 1.5 eV or more (Fig. Figure 8). The longest bondlengths and consequently smaller bond strengths are observed for Ta-N pairs which have a large number of Ta atoms in the surrounding. And opposite, the smallest bondlengths/largest bond strengths in the Ta-N pair are realized when Ti and Al atoms dominate in the vicinity of the pair. It is worth noting that the contribution of deep s-$d(e_g)$ hybridized states amounts of $\sim 1/3$ in the Ta-N bond strength in contrast to earlier claims that these states do not contribute to the bonding,[37,65] which were based on the DOS analysis only. The gain in metallicity of interatomic metal-nitrogen bonds in $Ti_{0.75-y}Al_{0.25}Ta_yN$ solutions with an increase in the concentration of tantalum is clearly seen from the distribution of the total valence

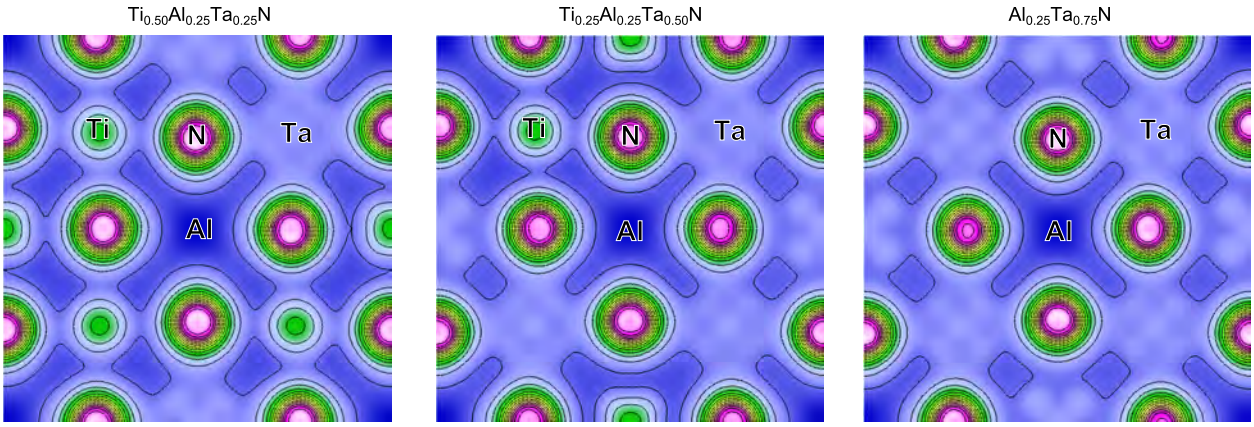

Figure 9: Charge density distribution in the (001) plane for $Ti_{0.75-y}Al_{0.25}Ta_yN$.

charge density (Fig. Figure 9). The metal-metal bonds in the quaternary solutions, like in parent TiN, are much weaker than the Me-N bonds. The average energy of metal-metal bond strength varies from ∼0.3 eV (Ti-Ti and Ti-Al bonds) to ∼0.9 eV (Ta-Ta bonds).

The change in the chemical bonding character in the $Ti_{0.75-y}Al_{0.25}Ta_yN$ system due to alloying with Ta also affects its elastic properties. For instance, $Ti_{0.50}Al_{0.25}Ta_{0.25}N$ (Fig. Figure 1), which can be considered as quaternary solution obtained from $Ti_{0.75}Al_{0.25}N$ by replacing of 0.25 titanium with tantalum, on the one hand, andas a result of replacing of 0.25 aluminum with tantalum in $Ti_{0.50}Al_{0.50}N$,, on the other hand, demonstrates an increase in the $\widetilde{C}_{11}$ elastic constant (by 7% and 17% regarding $Ti_{0.75}Al_{0.25}N$ and $Ti_{0.50}Al_{0.50}N$, respectively) and softening of the $\widetilde{C}_{12}$ and $\widetilde{C}_{44}$ constants. Moderate changes are observed for $\widetilde{C}_{12}$ (a 4% and 8% decrease with respect to $Ti_{0.75}Al_{0.25}N$ and $Ti_{0.50}Al_{0.50}N$), whereas the softening of $\widetilde{C}_{44}$ is more sizable. The latter elastic constant decreases by 20% and 34% as compared with $Ti_{0.75}Al_{0.25}N$ and $Ti_{0.50}Al_{0.50}N$, respectively. As a result, the Cauchy's pressure of $Ti_{0.50}Al_{0.25}Ta_{0.25}N$ becomes positive (10 GPa), and the B/G ratio decreases to 0.58. This indicates that already 25% alloying with Ta leads to a considerable increase in ductility of the TiN-based solutions. Thus, alloying with Ta is very effective in toughening the solutions that is in good agreement with experimental results[70] and is attributed not only to emerging Ta-Ta bonds, which primarily provide the metallic character of interatomic bonding in the quaternary solutions but also to the gain in metallicity of Ta-N bonds with increasing Ta concentration.

Conclusions

In summary, by using first-principles calculations we have examined quantitatively the chemical bonds in TiN and TiN-based ternary $Ti_{1-x}Al_xN$ and quaternary $Ti_{1-x-y}Al_xTa_yN$ solid solutions. The results show that alloying with aluminum on the titanium sublattice in TiN leads to the change in the Ti-N bond character from ionic to covalent, whereas emerging Al-N bonds in $Ti_{1-x}Al_xN$ are strongly ionic. Such alloying results in the linear decrease in the lattice parameter with growth of x, the displacements of Ti and N atoms from ideal positions and to variation in interatomic Ti-N bond lengths and bond strength energies, which can even exceed the bond energy in pure titanium nitride, although the average bond energy is reduced by 10–15%. The alloying with tantalum significantly reduces the ionicity of the Al-N bonds, while retaining the covalent character of the Ti-N bonds. At the same time, the quaternary solutions, which have larger variation in the pair Me-N bond lengths due to greater distortions of atomic positions from ideal sites of cubic lattice, demonstrate more considerable dispersion of the pair Me-N bond energies. Among them, the variation in energy of Ta-N bonds, which along with Ta-Ta bonds provides metallic character of the bonding in quaternary solutions, is even more significant. It is worth noting that according to COHP analysis the hybridization of deep lying s orbitals of N with $d(p)$ Me orbitals provides from 1/3 to 1/2 of the Me-N bond strength. Whereas in ternary $Ti_{1-x}Al_xN$ solutions the variation of Ti-N bond energy clearly correlates with the number of alloying atoms surrounding the Ti-N pair, in quaternary TiN-based solutions not only the number and type of neighboring alloying atoms, but their relative positioning affects the values of the bond energy in the pair. The obtained dependencies of the chemical bonding in $Ti_{1-x-y}Al_xTa_yN$ on on concentration and arrangement of alloying elements correlate well with changes in the elastic constants and agree with earlier established behavior of elastic properties of transition metal nitrides, which vary significantly with changing configurational order of metal atoms.[71]

Acknowledgement

We acknowledge the support by the Russian Science Foundation (Grant No. 18-19-00589) for DFT calculations and the Fundamental Research Program of the State Academies of Sciences, line of research III.23 in part of elastic properties analysis. Calculations were performed using computational resources provided by the SKIF-Cyberia supercomputer at the National Research Tomsk State University.

References

(1) Zhong, Y.; Xia, X.; Shi, F.; Zhan, J.; Tu, J.; Fan, H. J. Transition Metal Carbides and Nitrides in Energy Storage and Conversion. *Advanced Science* **2016**, *3*, 1500286.

(2) Johansson, L. I. Electronic and structural properties of transition-metal carbide and nitride surfaces. *Surface Science Reports* **1995**, *21*, 177 – 250.

(3) Vaz, F.; Machado, P.; Rebouta, L.; Cerqueira, P.; Goudeau, P.; Rivière, J.; Alves, E.; Pischow, K.; de Rijk, J. Mechanical characterization of reactively magnetron-sputtered TiN films. *Surface and Coatings Technology* **2003**, *174-175*, 375 – 382.

(4) Mayrhofer, P. H.; Mitterer, C.; Hultman, L.; Clemens, H. Microstructural design of hard coatings. *Progress in Materials Science* **2006**, *51*, 1032 – 1114.

(5) Savvides, N.; Window, B. Electrical transport, optical properties, and structure of TiN films synthesized by low-energy ion assisted deposition. *Journal of Applied Physics* **1988**, *64*, 225–234.

(6) Durusoy, H. Z.; Duyar, O.; Aydinli, A.; Ay, F. Influence of substrate temperature and bias voltage on the optical transmittance of TiN films. *Vacuum* **2003**, *70*, 21 – 28.

(7) Wu, L.; Yu, H. Y.; Li, X.; Pey, K. L.; Pan, J. S.; Chai, J. W.; Chiu, Y. S.; Lin, C. T.; Xu, J. H.; Wann, H. J.; Yu, X. F.; Lee, D. Y.; Hsu, K. Y.; Tao, H. J. Thermal stability of TiN metal gate

prepared by atomic layer deposition or physical vapor deposition on HfO_2 high-K dielectric. *Applied Physics Letters* **2010**, *96*, 113510.

(8) Khalifa, A. E.; Swillam, M. A. Cheap and efficient plasmonic solar cell. *Proc. SPIE* **2014**, *8981*, 89811R.

(9) Tanaka, T.; Nakajima, T.; Yamashita, K. Density functional study on the adsorption and surface reactions on SiO_2 in TiN-CVD using $TiCl_4$ and NH_3. *Thin Solid Films* **2002**, *409*, 51 – 57.

(10) Wang, J.; Liu, W.; Mei, T. The effect of thermal treatment on the electrical properties of titanium nitride thin films by filtered arc plasma method. *Ceramics International* **2004**, *30*, 1921 – 1924.

(11) Tang, D.; Yi, R.; Gordin, M. L.; Melnyk, M.; Dai, F.; Chen, S.; Song, J.; Wang, D. Titanium nitride coating to enhance the performance of silicon nanoparticles as a lithium-ion battery anode. *J. Mater. Chem. A* **2014**, *2*, 10375–10378.

(12) Balogun, M.-S.; Qiu, W.; Wang, W.; Fang, P.; Lu, X.; Tong, Y. Recent advances in metal nitrides as high-performance electrode materials for energy storage devices. *J. Mater. Chem. A* **2015**, *3*, 1364–1387.

(13) Zhang, M.; Garcia-Araez, N.; Hector, A. L.; Owen, J. R. A sol-gel route to titanium nitride conductive coatings on battery materials and performance of TiN-coated $LiFePO_4$. *J. Mater. Chem. A* **2017**, *5*, 2251–2260.

(14) Naik, G. V.; Schroeder, J. L.; Ni, X.; Kildishev, A. V.; Sands, T. D.; Boltasseva, A. Titanium nitride as a plasmonic material for visible and near-infrared wavelengths. *Opt. Mater. Express* **2012**, *2*, 478–489.

(15) Guler, U.; Naik, G. V.; Boltasseva, A.; Shalaev, V. M.; Kildishev, A. V. Performance analysis

of nitride alternative plasmonic materials for localized surface plasmon applications. *Applied Physics B* **2012**, *107*, 285–291.

(16) Naik, G. V.; Shalaev, V. M.; Boltasseva, A. Alternative Plasmonic Materials: Beyond Gold and Silver. *Advanced Materials* **2013**, *25*, 3264–3294.

(17) Guler, U.; Ndukaife, J. C.; Naik, G. V.; Nnanna, A. G. A.; Kildishev, A. V.; Shalaev, V. M.; Boltasseva, A. Local Heating with Lithographically Fabricated Plasmonic Titanium Nitride Nanoparticles. *Nano Letters* **2013**, *13*, 6078–6083.

(18) Naik, G. V.; Saha, B.; Liu, J.; Saber, S. M.; Stach, E. A.; Irudayaraj, J. M. K.; Sands, T. D.; Shalaev, V. M.; Boltasseva, A. Epitaxial superlattices with titanium nitride as a plasmonic component for optical hyperbolic metamaterials. *Proceedings of the National Academy of Sciences* **2014**, *111*, 7546–7551.

(19) Wang, D.-Y.; Chiu, M.-C. Characterization of TiN coatings post-treated by metal-plasma ion implantation process. *Surface and Coatings Technology* **2002**, *156*, 201 – 207.

(20) Chim, Y.; Ding, X.; Zeng, X.; Zhang, S. Oxidation resistance of TiN, CrN, TiAlN and CrAlN coatings deposited by lateral rotating cathode arc. *Thin Solid Films* **2009**, *517*, 4845 – 4849.

(21) Madan, A.; Kim, I. W.; Cheng, S. C.; Yashar, P.; Dravid, V. P.; Barnett, S. A. Stabilization of Cubic AlN in Epitaxial AlN/TiN Superlattices. *Phys. Rev. Lett.* **1997**, *78*, 1743–1746.

(22) PalDey, S.; Deevi, S. C. Single layer and multilayer wear resistant coatings of (Ti,Al)N: a review. *Materials Science and Engineering: A* **2003**, *342*, 58–79.

(23) Liu, Z.-J.; Shum, P.; Shen, Y. Hardening mechanisms of nanocrystalline Ti-Al-N solid solution films. *Thin Solid Films* **2004**, *468*, 161 – 166.

(24) Carvalho, S.; Ribeiro, E.; Rebouta, L.; Pacaud, J.; Goudeau, P.; Renault, P.; Rivière, J.; Tavares, C. PVD grown (Ti,Si,Al)N nanocomposite coatings and (Ti,Al)N/(Ti,Si)N

multilayers: structural and mechanical properties. *Surface and Coatings Technology* **2003**, *172*, 109 – 116.

(25) Godinho, V.; Philippon, D.; Rojas, T.; Novikova, N.; Yakovlev, V.; Vinogradov, E.; Fernandez, A. Characterization of $Ti_{1-x}Al_xN$ coatings with selective IR reflectivity. *Solar Energy* **2010**, *84*, 1397 – 1401.

(26) Schüler, A.; Thommen, V.; Reimann, P.; Oelhafen, P.; Francz, G.; Zehnder, T.; Düggelin, M.; Mathys, D.; Guggenheim, R. Structural and optical properties of titanium aluminum nitride films ($Ti_{1-x}Al_xN$). *Journal of Vacuum Science and Technology, Part A: Vacuum, Surfaces and Films* **2001**, *19*, 922–929.

(27) Sedighi, M.; Padilla, R. V.; Taylor, R. A.; Lake, M.; Izadgoshasb, I.; Rose, A. High-temperature, point-focus, pressurised gas-phase solar receivers: A comprehensive review. *Energy Conversion and Management* **2019**, *185*, 678 – 717.

(28) Rachbauer, R.; Massl, S.; Stergar, E.; Holec, D.; Kiener, D.; Keckes, J.; Patscheider, J.; Stiefel, M.; Leitner, H.; Mayrhofer, P. H. Decomposition pathways in age hardening of Ti-Al-N films. *Journal of Applied Physics* **2011**, *110*, 023515.

(29) Chen, L.; Holec, D.; Du, Y.; Mayrhofer, P. H. Influence of Zr on structure, mechanical and thermal properties of Ti-Al-N. *Thin Solid Films* **2011**, *519*, 5503 – 5510.

(30) Meindlhumer, M.; Zalesak, J.; Pitonak, R.; Todt, J.; Sartory, B.; Burghammer, M.; Stark, A.; Schell, N.; Daniel, R.; Keckes, J. F.; Lessiak, M.; Köpf, A.; Weißenbacher, R.; Keckes, J. Biomimetic hard and tough nanoceramic Ti-Al-N film with self-assembled six-level hierarchy. *Nanoscale* **2019**, *11*, 7986–7995.

(31) Shugurov, A. R.; Kazachenok, M. S. Mechanical properties and tribological behavior of magnetron sputtered TiAlN/TiAl multilayer coatings. *Surface and Coatings Technology* **2018**, *353*, 254 – 262.

(32) Yang, Y.; Xu, Y. X.; Chen, L.; Mayrhofer, P. H. Improved Ti-Al-N coatings through Ta alloying and multilayer architecture. *Surface and Coatings Technology* **2017**, *328*, 428 – 435.

(33) Lind, H.; Forsén, R.; Alling, B.; Ghafoor, N.; Tasnádi, F.; Johansson, M. P.; Abrikosov, I. A.; Odén, M. Improving thermal stability of hard coating films via a concept of multicomponent alloying. *Applied Physics Letters* **2011**, *99*, 091903.

(34) Glatz, S.; Hollerweger, R.; Polcik, P.; Rachbauer, R.; Paulitsch, J.; Mayrhofer, P. Thermal stability and mechanical properties of arc evaporated Ti-Al-Zr-N hard coatings. *Surface and Coatings Technology* **2015**, *266*, 1 – 9.

(35) Mikula, M.; Plašienka, D.; Sangiovanni, D. G.; Sahul, M.; Roch, T.; Truchlý, M.; Gregor, M.; Čaplovič, L.; Plecenik, A.; Kúš, P. Toughness enhancement in highly NbN-alloyed Ti-Al-N hard coatings. *Acta Materialia* **2016**, *121*, 59 – 67.

(36) Xu, Y. X.; Chen, L.; Pei, F.; Du, Y.; Liu, Y.; Yue, J. L. Influence of Hf on the structure, thermal stability and oxidation resistance of Ti-Al-N coatings. *Thin Solid Films* **2014**, *565*, 25 – 31.

(37) Rachbauer, R.; Holec, D.; Mayrhofer, P. Increased thermal stability of Ti-Al-N thin films by Ta alloying. *Surface and Coatings Technology* **2012**, *211*, 98 – 103.

(38) Hollerweger, R.; Riedl, H.; Paulitsch, J.; Arndt, M.; Rachbauer, R.; Polcik, P.; Primig, S.; Mayrhofer, P. Origin of high temperature oxidation resistance of Ti-Al-Ta-N coatings. *Surface and Coatings Technology* **2014**, *257*, 78 – 86.

(39) Shugurov, A. R.; Akulinkin, A. A.; Kasterov, A. M.; Kalashnikov, M. P. The Influence of Nitrogen Partial Pressure on the Composition, Microstructure, and Mechanical Characteristics of $Ti_{1-x-y}Al_xTa_yN$ Coatings Obtained by Reactive Magnetron Sputtering. *Technical Physics Letters* **2019**, *45*, 418–422.

(40) Mikula, M.; Truchlý, M.; Sangiovanni, D. G.; Plašienka, D.; Roch, T.; Gregor, M.; Ďurina, P.; Janik, M.; Kúš, P. Experimental and computational studies on toughness enhancement in Ti-Al-Ta-N quaternaries. *Journal of Vacuum Science & Technology A* **2017**, *35*, 060602.

(41) Rahman, M. M.; Jiang, Z.-T.; Munroe, P.; Chuah, L. S.; Zhou, Z.-f.; Xie, Z.; Yin, C. Y.; Ibrahim, K.; Amri, A.; Kabir, H.; Haque, M. M.; Mondinos, N.; Altarawneh, M.; Dlugogorski, B. Z. Chemical bonding states and solar selective characteristics of unbalanced magnetron sputtered $Ti_xM_{1-x-y}N_y$ films. *RSC Adv.* **2016**, *6*, 36373–36383.

(42) Barshilia, H. C.; Selvakumar, N.; Rajam, K.; Biswas, A. Optical properties and thermal stability of TiAlN/AlON tandem absorber prepared by reactive DC/RF magnetron sputtering. *Solar Energy Materials and Solar Cells* **2008**, *92*, 1425 – 1433.

(43) Kuang, H.; Tan, D.; He, W.; Yi, Z.; Yuan, F.; Xu, Y. Oxidation behavior of the TiAlN hard coating in the process of recycling coated hardmetal scrap. *RSC Adv.* **2019**, *9*, 14503–14510.

(44) Serro, A.; Completo, C.; Colaço, R.; dos Santos, F.; da Silva, C. L.; Cabral, J.; Araújo, H.; Pires, E.; Saramago, B. A comparative study of titanium nitrides, TiN, TiNbN and TiCN, as coatings for biomedical applications. *Surface and Coatings Technology* **2009**, *203*, 3701 – 3707.

(45) Esguerra-Arce, A.; Esguerra-Arce, J.; Yate, L.; Amaya, C.; Coy, L. E.; Aguilar, Y.; Gutiérrez, O.; Moya, S. Influence of the Al content on the *in vitro* bioactivity and biocompatibility of PVD $Ti_{1-x}Al_xN$ coatings for orthopaedic applications. *RSC Adv.* **2016**, *6*, 60756–60764.

(46) Mayrhofer, P. H.; Hörling, A.; Karlsson, L.; Sjölén, J.; Larsson, T.; Mitterer, C.; Hultman, L. Self-organized nanostructures in the Ti-Al-N system. *Applied Physics Letters* **2003**, *83*, 2049–2051.

(47) Holec, D.; Rachbauer, R.; Chen, L.; Wang, L.; Luef, D.; Mayrhofer, P. H. Phase stability and

alloy-related trends in Ti-Al-N, Zr-Al-N and Hf-Al-N systems from first principles. *Surface and Coatings Technology* **2011**, *206*, 1698 – 1704.

(48) Tasnádi, F.; Rogström, L.; Zhu, J.; Wang, F.; Hsu, T.-W.; Lind, H.; Abrikosov, I.; Johansson-Jõesaar, M.; Odén, M. High temperature thermodynamics of spinodal decomposition in arc deposited $Ti_xNb_yAl_zN$ coatings. *Materials & Design* **2018**, *150*, 165 – 170.

(49) Chen, Y.; Roa, J.; Yu, C.; Johansson-Jõesaar, M.; Andersson, J.; Anglada, M.; Odén, M.; Rogström, L. Enhanced thermal stability and fracture toughness of TiAlN coatings by Cr, Nb and V-alloying. *Surface and Coatings Technology* **2018**, *342*, 85 – 93.

(50) Momma, K.; Izumi, F. LOBSTER: A tool to extract chemical bonding from plane-wave based DFT. *Journal of Computational Chemistry* **2016**, *37*, 1030–1035.

(51) Kresse, G.; Hafner, J. Ab initio molecular dynamics for open-shell transition metals. *Phys. Rev. B* **1993**, *48*, 13115–13118.

(52) Kresse, G.; Furthmüller, J. Efficient iterative schemes for ab initio total-energy calculations using a plane-wave basis set. *Phys. Rev. B* **1996**, *54*, 11169–11186.

(53) Blöchl, P. E. Projector augmented-wave method. *Phys. Rev. B* **1994**, *50*, 17953–17979.

(54) Kresse, G.; Joubert, D. From ultrasoft pseudopotentials to the projector augmented-wave method. *Phys. Rev. B* **1999**, *59*, 1758–1775.

(55) Perdew, J. P.; Burke, K.; Ernzerhof, M. Generalized Gradient Approximation Made Simple. *Phys. Rev. Lett.* **1996**, *77*, 3865–3868.

(56) Le Page, Y.; Saxe, P. Symmetry-general least-squares extraction of elastic data for strained materials from ab initio calculations of stress. *Phys. Rev. B* **2002**, *65*, 104104.

(57) Wu, X.; Vanderbilt, D.; Hamann, D. R. Systematic treatment of displacements, strains, and electric fields in density-functional perturbation theory. *Phys. Rev. B* **2005**, *72*, 035105.

(58) Li, X.-q.; Zhao, J.-j.; Xu, J.-c. Mechanical properties of bcc Fe-Cr alloys by first-principles simulations. *Frontiers of Physics* **2012**, *7*, 360–365.

(59) Dronskowski, R.; Bloechl, P. E. Crystal orbital Hamilton populations (COHP): energy-resolved visualization of chemical bonding in solids based on density-functional calculations. *The Journal of Physical Chemistry* **1993**, *97*, 8617–8624.

(60) Deringer, V. L.; Tchougréeff, A. L.; Dronskowski, R. Crystal Orbital Hamilton Population (COHP) Analysis As Projected from Plane-Wave Basis Sets. *The Journal of Physical Chemistry A* **2011**, *115*, 5461–5466.

(61) Maintz, S.; Deringer, V. L.; Tchougréeff, A. L.; Dronskowski, R. Analytic projection from plane-wave and PAW wavefunctions and application to chemical-bonding analysis in solids. *Journal of Computational Chemistry* **2013**, *34*, 2557–2567.

(62) Maintz, S.; Deringer, V. L.; Tchougréeff, A. L.; Dronskowski, R. LOBSTER: A tool to extract chemical bonding from plane-wave based DFT. *Journal of Computational Chemistry* **2016**, *37*, 1030–1035.

(63) Brager, A. An X-ray examination of titanium nitride III. *Acta Physicochimica* **1939**, *9*, 617 – 632.

(64) Kim, J. O.; Achenbach, J. D.; Mirkarimi, P. B.; Shinn, M.; Barnett, S. A. Elastic constants of single-crystal transition-metal nitride films measured by line-focus acoustic microscopy. *Journal of Applied Physics* **1992**, *72*, 1805–1811.

(65) Matenoglou, G. M.; Lekka, C. E.; Koutsokeras, L. E.; Karras, G.; Kosmidis, C.; Evangelakis, G. A.; Patsalas, P. Structure and electronic properties of conducting, ternary $Ti_xTa_{1-x}N$ films. *Journal of Applied Physics* **2009**, *105*, 103714.

(66) Sangiovanni, D. G.; Chirita, V.; Hultman, L. Electronic mechanism for toughness enhancement in $Ti_xM_{1-x}N$ (M = Mo and W). *Phys. Rev. B* **2010**, *81*, 104107.

(67) Tang, W.; Sanville, E.; Henkelman, G. A grid-based Bader analysis algorithm without lattice bias. *Journal of Physics: Condensed Matter* **2009**, *21*, 084204.

(68) Pettifor, D. G. Theoretical predictions of structure and related properties of intermetallics. *Materials Science and Technology* **1992**, *8*, 345–349.

(69) Pugh, S. XCII. Relations between the elastic moduli and the plastic properties of polycrystalline pure metals. *The London, Edinburgh, and Dublin Philosophical Magazine and Journal of Science* **1954**, *45*, 823–843.

(70) Seidl, W.; Bartosik, M.; Kolozsvári, S.; Bolvardi, H.; Mayrhofer, P. Influence of Ta on the fracture toughness of arc evaporated Ti-Al-N. *Vacuum* **2018**, *150*, 24 – 28.

(71) Edström, D.; Sangiovanni, D.; Hultman, L.; Chirita, V. Effects of atomic ordering on the elastic properties of TiN- and VN-based ternary alloys. *Thin Solid Films* **2014**, *571*, 145 – 153.